CEAS-GNC-2022-028

CEAS EuroGNC 2022
"Conference on Guidance, Navigation and Control"
3-5 May 2022 @ Technische Universität Berlin, Germany

Spacecraft Rendezvous Hovering Predictive Control around a Near-Rectilinear Halo Orbit

Julio C. Sanchez Ph.D. Candidate, Universidad de Sevilla, Aerospace Engineering Department, 41092, Sevilla, Spain. jsanchezm@us.es

Francisco Gavilan Assistant Professor, Universidad de Sevilla, Aerospace Engineering Department, 41092, Sevilla, Spain. fgavilan@us.es

Rafael Vazquez Associate Professor, Universidad de Sevilla, Aerospace Engineering Department, 41092, Sevilla, Spain. rvazquez1@us.es

Christophe Louembet Associate Professor, Laboratoire d'analyse et d'architecture des systèmes, Methods and Algorithms in Control, 31400, Toulouse, France. louembet@laas.fr

ABSTRACT

In this paper the spacecraft rendezvous hovering phase, under circular restricted three-body problem assumptions, is addressed. The objective is to stay close to a Near-Rectilinear Halo Orbit, similar to the one proposed for the future Lunar Orbital Platform-Gateway. The relative dynamics are linearized assuming the vehicles are close enough. Then, a simplified propagation method based on assuming the state matrix as constant is developed. This allows to obtain an analytical approximate solution based on the state matrix eigendecomposition. Using this propagation model, the hovering phase problem is posed and recast as a static program. This static program is solved periodically to update the required control sequence. The numerical results demonstrate the efficiency of the proposed propagation method and the hovering phase mission fulfilment.

Keywords: Linear-time varying systems; Spacecraft control; Three-body problem.

Nomenclature

D	=	Distance between primaries
I	=	Inertial frame
$\mathbf{r}$	=	Absolute position
S	=	Synodic frame
t	=	Time
$\Delta\mathbf{V}$	=	Velocity increment
$\mathbf{x}$	=	Relative state
θ	=	Phase angle
μ	=	Standard gravitational parameter
$\boldsymbol{\rho}$	=	Relative position
$\boldsymbol{\Phi}$	=	State transition matrix
$\boldsymbol{\omega}$	=	Angular velocity

Except where otherwise noted, content of this paper is licensed under a Creative Commons Attribution 4.0 International License.

The reproduction and distribution with attribution of the entire paper or of individual pages, in electronic or printed form, including some materials under non-CC-BY 4.0 licenses is hereby granted by the respective copyright owners.

1 Introduction

Demonstrating autonomous close proximity operations under the three-body problem context is gaining attention recently, a key reason being that International Space Station partners plan to build a space station, named Lunar Orbital Platform Gateway (LOP-G), in the cislunar space (see Ref. [1]).

The preferred option to place the LOP-G is a southern Near Rectilinear Halo Orbit (NRHO) around the L_2 Earth-Moon system equilibrium (see Ref. [2]). This is due to the evidence of ice presence at the Moon south pole (see Ref. [3]), and the possibility of observing the far side of the Moon. The NRHOs are members of the broader set of the L_1 and L_2 halos families arising in the circular restricted three-body problem (CRTBP). The NRHOs present also favourable stability properties, thus reducing station-keeping needs (see Ref. [4]).

When applied to space operations, the CRTBP literature has mainly focused on exploiting the orbit invariant manifolds to obtain low energy transfers (see Ref. [5, 6]). However, close proximity operations require to explicitly take into account the relative motion between the two vehicles. Some recent works have addressed this topic. Reference [7] described the relative dynamics in a local frame attached to the target, Ref. [8] implemented a close rendezvous strategy based on line-of-sight hold points and Ref. [9] developed a chance-constrained model predictive controller (MPC) to ensure robust line-of-sight constraints satisfaction.

In the context of spacecraft rendezvous, the hovering phase consists on a spacecraft maintaining its relative position with respect to a known location (e.g. a leader vehicle). This mission phase has been largely addressed under Keplerian assumptions (see Ref. [10, 11]). However, as far as the authors know, hovering phase strategies under the CRTBP have not been studied. The objective of this work is to provide a control strategy for the CRTBP hovering phase. The main assumption is that the leader vehicle evolves naturally in a periodic orbit whereas the follower is equipped with chemical thrusters. Consequently, the control action is considered to be impulsive. Some relevant works on impulsive close proximity operations, under Keplerian assumptions, can be found in Ref. [12] where passive safe trajectories are designed, Ref. [13] where a MPC is presented to handle disturbances and Ref. [14] transformed the rendezvous problem into an asymptotic stabilization of a switching system.

This paper linearizes the CRTBP relative dynamics assuming the vehicles are close enough ($\sim$ 1 km). However, for a leader evolving in a periodic orbit, the resulting system is linear time-varying (LTV). Additionally, CRTBP orbits are described in terms of discrete numerical positions and velocities (see Ref. [15]), without any analytical representation available. This fact precludes the obtention of a closed-form expression for the state transition matrix (STM) as in the Keplerian problem (see Ref. [16]). An approach to obtain the STM could be numerical integration (see Ref. [9]). However, this augments computational burden. To solve this issue, this work proposes a novel approach by assuming the system as linear time-invariant (LTI) for a short propagation period (the target position is considered stationary). This allows to conveniently express the relative state in terms of the state matrix eigendecomposition. When the propagation interval ends, the leader position is updated and the state matrix eigendecomposition is computed again. This approach reduces the computational burden with only a small loss of accuracy and provides some information about the relative state solution structure.

Using the exact solution of the approximate dynamics, discretization and a compact formulation, the continuous hovering problem is transformed into a finite tractable static program. The result is a linear programming (LP) problem which is efficient to solve. This allows to sequentially update the control sequence in an MPC fashion (see Ref. [17]) to account for non-linearities and discretization errors.

The structure of the paper is as follows. Section II presents the CRTBP relative motion and its linearization. The propagation models for the linearized system are presented in Section III. Section IV states the hovering problem and recasts it to LP form. Section V presents numerical results of interest. Finally, Section VI concludes the paper with some additional remarks

Except where otherwise noted, content of this paper is licensed under a Creative Commons Attribution 4.0 International License.

The reproduction and distribution with attribution of the entire paper or of individual pages, in electronic or printed form, including some materials under non-CC-BY 4.0 licenses is hereby granted by the respective copyright owners.

2 CRTBP relative motion

In this section, the linear relative motion model is derived. Firstly, the CRTBP assumptions are presented. Then, the relative motion dynamics between two vehicles is obtained. Finally, the gravitational terms are linearized assuming the two vehicles are close enough.

2.1 CRTBP dynamics

Under CRTBP assumptions, i.e., $M_1 > M_2 \gg m$ (being M_1, M_2 the primaries' masses and m the spacecraft mass) and a constant distance D between primaries, the spacecraft dynamics can be expressed in the synodic frame. Denote the inertial frame by $I : \{\mathbf{O}, \mathbf{i}_I, \mathbf{j}_I, \mathbf{k}_I\}$ where $\mathbf{O}$ is the system barycenter position. Denote the synodic frame by $S : \{\mathbf{O}, \mathbf{i}_S, \mathbf{j}_S, \mathbf{k}_S\}$ with $\mathbf{i}_S$ coincident with the line uniting the two primaries (positive towards the second primary), $\mathbf{k}_S$ parallel to the system kinetic momentum and $\mathbf{j}_S$ closing the right-handed system, see Fig.1. Then, the CRTBP dynamics, in frame S, is

$$\ddot{\mathbf{r}} + 2\boldsymbol{\omega} \times \dot{\mathbf{r}} + \boldsymbol{\omega} \times (\boldsymbol{\omega} \times \mathbf{r}) = -\mu_1 \frac{\mathbf{r} - \mathbf{r}_1}{||\mathbf{r} - \mathbf{r}_1||_2^3} - \mu_2 \frac{\mathbf{r} - \mathbf{r}_2}{||\mathbf{r} - \mathbf{r}_2||_2^3}, \tag{1}$$

where $\mathbf{r} = [x, y, z]^T$ is the spacecraft position, $\mathbf{r}_1 = [-\mu D, 0, 0]^T$ is the first primary position, $\mathbf{r}_2 = [(1-\mu)D, 0, 0]^T$ is the second primary position, $\boldsymbol{\omega} = [0, 0, \sqrt{(\mu_1 + \mu_2)/D^3}]^T$ is the angular velocity of the synodic frame with respect to the inertial and $\mu = \mu_2/(\mu_1 + \mu_2)$ is the primaries mass-ratio parameter.

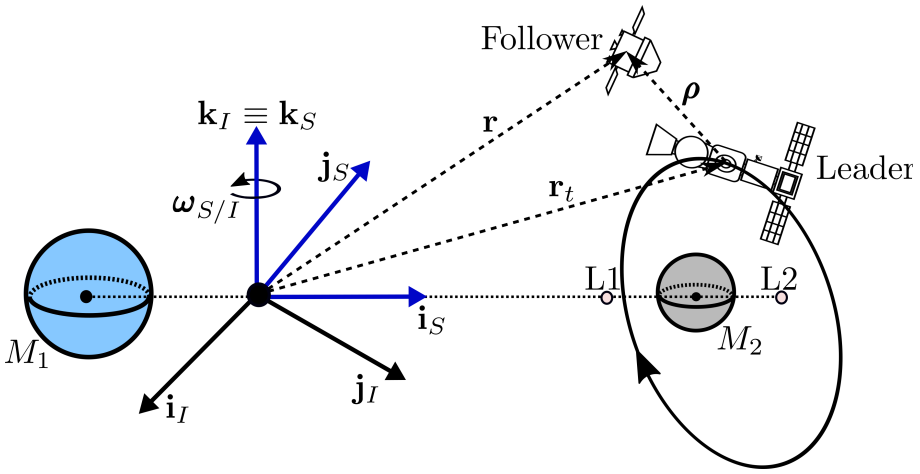

Fig. 1 Inertial and synodic frames of reference

2.2 Relative motion

Asssume a leader spacecraft and a follower with their positions given by $\mathbf{r}_t$ and $\mathbf{r}$, respectively. The relative position between the vehicles is $\boldsymbol{\rho} = \mathbf{r} - \mathbf{r}_t = [\Delta x, \Delta y, \Delta z]^T$. The relative dynamics is

$$\ddot{\boldsymbol{\rho}} + 2\boldsymbol{\omega} \times \dot{\boldsymbol{\rho}} + \boldsymbol{\omega} \times (\boldsymbol{\omega} \times \boldsymbol{\rho}) = -\mu_1 \left(\frac{\boldsymbol{\rho} + \mathbf{r}_{1t}}{||\boldsymbol{\rho} + \mathbf{r}_{1t}||_2^3} - \frac{\mathbf{r}_{1t}}{||\mathbf{r}_{1t}||_2^3} \right) - \mu_2 \left(\frac{\boldsymbol{\rho} + \mathbf{r}_{2t}}{||\boldsymbol{\rho} + \mathbf{r}_{2t}||_2^3} - \frac{\mathbf{r}_{2t}}{||\mathbf{r}_{2t}||_2^3} \right), \tag{2}$$

where $\mathbf{r}_{1t} = \mathbf{r}_t - \mathbf{r}_1$, $\mathbf{r}_{2t} = \mathbf{r}_t - \mathbf{r}_2$ and the leader position evolution $\mathbf{r}_t$ is assumed to be known.

Except where otherwise noted, content of this paper is licensed under a Creative Commons Attribution 4.0 International License.

The reproduction and distribution with attribution of the entire paper or of individual pages, in electronic or printed form, including some materials under non-CC-BY 4.0 licenses is hereby granted by the respective copyright owners.

2.3 Linearized relative motion

In this work, close proximity operations are considered, hence $||\mathbf{r}_{1t}||_2, ||\mathbf{r}_{2t}||_2 \gg ||\boldsymbol{\rho}||_2$. This allows the linearization of Eq. (2) considering

$$\frac{\mathbf{r}_{it}+\boldsymbol{\rho}}{||\mathbf{r}_{it}+\boldsymbol{\rho}||_2^3} \approx \frac{\mathbf{r}_{it}}{r_{it}^3} + \frac{1}{r_{it}^3}\left(\mathbf{I} - 3\frac{\mathbf{r}_{it}\mathbf{r}_{it}^T}{r_{it}^2}\right)\boldsymbol{\rho}, \quad i = 1,2, \tag{3}$$

where the linearization point is $\boldsymbol{\rho} \approx \mathbf{0}$. Introducing the linearization of Eq. (3) into Eq. (2)

$$\ddot{\boldsymbol{\rho}} = -\left[\boldsymbol{\Omega}^2 + \frac{\mu_1}{r_{1t}^3}\left(\mathbf{I} - 3\frac{\mathbf{r}_{1t}\mathbf{r}_{1t}^T}{r_{1t}^2}\right) + \frac{\mu_2}{r_{2t}^3}\left(\mathbf{I} - 3\frac{\mathbf{r}_{2t}\mathbf{r}_{2t}^T}{r_{2t}^2}\right).\right]\boldsymbol{\rho} - 2\boldsymbol{\Omega}\dot{\boldsymbol{\rho}}, \tag{4}$$

Note that the matrix $\boldsymbol{\Omega}$ denotes the cross product (algebraically) associated to $\boldsymbol{\omega}$ and let also define the matrix $\boldsymbol{\Sigma}(t)$ which collects the linearized gravitational terms of Eq. (4)

$$\boldsymbol{\Omega} = \begin{bmatrix} 0 & -\omega & 0 \\ \omega & 0 & 0 \\ 0 & 0 & 0 \end{bmatrix}, \qquad \boldsymbol{\Sigma}(t) = -\frac{\mu_1}{r_{1t}^3}\left(\mathbf{I} - 3\frac{\mathbf{r}_{1t}\mathbf{r}_{1t}^T}{r_{1t}^2}\right) - \frac{\mu_2}{r_{2t}^3}\left(\mathbf{I} - 3\frac{\mathbf{r}_{2t}\mathbf{r}_{2t}^T}{r_{2t}^2}\right), \tag{5}$$

then, the linearized motion of Eq. (4) can be stated as a LTV system as follows

$$\begin{bmatrix} \dot{\boldsymbol{\rho}} \\ \ddot{\boldsymbol{\rho}} \end{bmatrix} = \begin{bmatrix} \mathbf{0} & \mathbf{I} \\ -\boldsymbol{\Omega}^2 + \boldsymbol{\Sigma}(t) & -2\boldsymbol{\Omega} \end{bmatrix} \begin{bmatrix} \boldsymbol{\rho} \\ \dot{\boldsymbol{\rho}} \end{bmatrix}, \tag{6}$$

.

3 Propagation models

The leader lies in a CRTBP periodic orbit (numerically computed) around an equilibria (see Fig. 2). This causes the matrix $\boldsymbol{\Sigma}(t)$ to be time dependant, hence the system evolution as per Eq. (6) is LTV and not easy to solve. In this section, two propagation models are presented. The first one relies on numerical

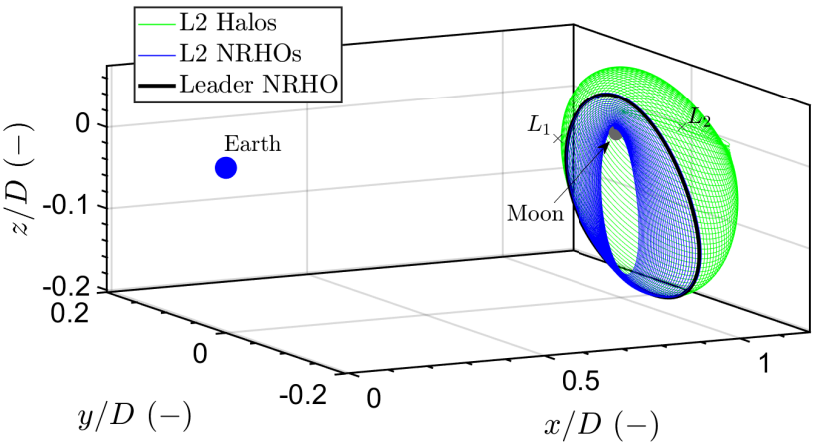

Fig. 2 Illustration of Southern L2 Halos in the Earth-Moon system.

integration to obtain the state transition matrix. The second one considers the target position as constant during a small propagation interval which allows to express the solution in terms of the state matrix eigendecomposition.

Except where otherwise noted, content of this paper is licensed under a Creative Commons Attribution 4.0 International License.

The reproduction and distribution with attribution of the entire paper or of individual pages, in electronic or printed form, including some materials under non-CC-BY 4.0 licenses is hereby granted by the respective copyright owners.

3.1 STM integration

Let define the relative state as $\mathbf{x} = [\boldsymbol{\rho}^T, \dot{\boldsymbol{\rho}}^T]^T$, then Eq. (6) is of the form $\dot{\mathbf{x}}(t) = \mathbf{A}(t)\mathbf{x}(t)$. The solution to the previous system can be expressed as $\mathbf{x}(t) = \boldsymbol{\Phi}(t,t_0)\mathbf{x}_0$ where $\boldsymbol{\Phi}(t,t_0)$ is the state transition matrix from t_0 to t which evolves as

$$\dot{\boldsymbol{\Phi}}(t,t_0) = \mathbf{A}(t)\boldsymbol{\Phi}(t,t_0), \quad \boldsymbol{\Phi}(t_0,t_0) = \mathbf{I}. \tag{7}$$

Note that Eq. (7) is a first order ODE composed of 36 equations.

3.2 Zero-order hold approach

An alternative approach to propagate Eq. (6) consists in assuming the target position as constant $\mathbf{r}_t$ during a small interval of duration ΔT. Then, the matrix $\mathbf{A}$ becomes time-invariant, along ΔT:

$$\mathbf{A} = \begin{bmatrix} 0 & 0 & 0 & 1 & 0 & 0 \\ 0 & 0 & 0 & 0 & 1 & 0 \\ 0 & 0 & 0 & 0 & 0 & 1 \\ \omega^2 + c_{xx} & c_{xy} & c_{xz} & 0 & 2\omega & 0 \\ c_{xy} & \omega^2 + c_{yy} & c_{yz} & -2\omega & 0 & 0 \\ c_{xz} & c_{yz} & c_{zz} & 0 & 0 & 0 \end{bmatrix}, \tag{8}$$

where the coefficients $c_{xx}, c_{yy}, c_{zz}, c_{xy}, c_{xz}, c_{yz} \equiv f(\mathbf{r}_t)$. In general, a coupling arises between xy and z. This coupling only vanishes for $\mathbf{r}_t$ along the x axis, e.g. collinear equilibria. Then, the solution to the system $\dot{\mathbf{x}}(t) = \mathbf{A}\mathbf{x}(t)$ can be expressed in terms of the $\mathbf{A}$ eigendecomposition

$$\mathbf{x}(t) = \sum_{j=1}^{6} d_j e^{\lambda_j (t-t_0)} \mathbf{v}_j, \tag{9}$$

where λ_j are the eigenvalues, $\mathbf{v}_j$ the eigenvectors and d_j the integration constants. It can be demonstrated that the eigenvalues structure along a halo orbit yields two pure real eigenvalues ($\lambda_1, \lambda_2 \in \mathbb{R}$) and two pure imaginary pairs ($\lambda_3 = n_1 i$, $\lambda_4 = n_2 i$, $\lambda_5 = \overline{\lambda}_3$, $\lambda_6 = \overline{\lambda}_4$, $n_1, n_2 \in \mathbb{R}$) as it will be shown in Fig. 5. As a consequence, Eq. (9) can be expanded as

$$\begin{aligned} \mathbf{x}(t) =& d_1 \mathbf{v}_1 e^{\lambda_1 \Delta t} + d_2 \mathbf{v}_2 e^{\lambda_2 \Delta t} + d_3(\mathbf{v}_3 \cos(n_1 \Delta t) - \mathbf{v}_4 \sin(n_1 \Delta t)) + d_4(\mathbf{v}_4 \cos(n_1 \Delta t) + \mathbf{v}_3 \sin(n_1 \Delta t)) \\ &+ d_5(\mathbf{v}_5 \cos(n_2 \Delta t) - \mathbf{v}_6 \sin(n_2 \Delta t)) + d_6(\mathbf{v}_6 \cos(n_2 \Delta t) + \mathbf{v}_5 \sin(n_2 \Delta t)), \end{aligned} \tag{10}$$

where $\lambda_1, n_1, n_2 > 0$, $\lambda_2 < 0$ and $\Delta t = t - t_0$. Note that the unstable behaviour is associated to d_1.

4 Impulsive hovering phase

The aim of this section is to present the hovering control problem and a numerical method to solve it. The control action is considered as impulsive which models with adequate accuracy a chemical thruster. When an impulse is applied the state changes instantaneously as

$$\mathbf{x}^+(t) = \mathbf{x}(t) + \mathbf{B}\Delta\mathbf{V}(t), \tag{11}$$

where the superscript $^+$ represents the state after the impulse, $\Delta\mathbf{V} = [\Delta V_x, \Delta V_y, \Delta V_z]^T$ is the applied impulse and the control matrix is given by $\mathbf{B} = [\mathbf{0}, \mathbf{I}]^T$.

Except where otherwise noted, content of this paper is licensed under a Creative Commons Attribution 4.0 International License.

The reproduction and distribution with attribution of the entire paper or of individual pages, in electronic or printed form, including some materials under non-CC-BY 4.0 licenses is hereby granted by the respective copyright owners.

4.1 Problem statement

The objective of the hovering phase is to maintain the follower vehicle within a prescribed space subset. This hovering region can be described, without loss of generality, by a cuboid

$$\underline{\Delta x} \leq \Delta x(t) \leq \overline{\Delta x}, \quad \underline{\Delta y} \leq \Delta y(t) \leq \overline{\Delta y}, \quad \underline{\Delta z} \leq \Delta z(t) \leq \overline{\Delta z}. \tag{12}$$

The hovering problem is stated as

$$\begin{aligned} \min_{\mathbf{x}(t),\Delta\mathbf{V}(t)} \quad & \int_{t_0}^{t_f} ||\Delta\mathbf{V}(t)||_1 dt, \\ \text{s.t.} \quad & \dot{\mathbf{x}}(t) = \mathbf{A}(t)\mathbf{x}(t), \\ & \mathbf{x}^+(t) = \mathbf{x}(t) + \mathbf{B}\Delta\mathbf{V}(t), \\ & \mathbf{A}_{\text{hov}}\mathbf{x}(t) \leq \mathbf{b}_{\text{hov}}, \\ & -\overline{\Delta\mathbf{V}} \leq \Delta\mathbf{V}(t) \leq \overline{\Delta\mathbf{V}}, \\ & \mathbf{x}(t_0) = \mathbf{x}_0, \end{aligned} \tag{13}$$

where $\mathbf{A}_{\text{hov}} \in \mathbb{R}^{6\times 6}$ and $\mathbf{b}_{\text{hov}} \in \mathbb{R}^6$ define the hovering region constraints of Eq. (12). Problem (13) has infinite degrees of freedom since the impulses can be placed anywhere.

4.2 Static program

The continuous optimization problem (13) is converted to a finite tractable static program by means of discretization. Assume N impulses, $\Delta\mathbf{V}_k$, equispaced along the hovering phase at times $t_k = t_0 + (k-1)\Delta t$ with $\Delta t = (t_f - t_0)/N$. Thus, the impulses take place at the beginning of the intervals. Using the zero-order hold approach given by Eq. (10) and updating the constant matrix $\mathbf{A}$ for each interval between impulses, the state propagation depends on the integration constants of each interval $\mathbf{d}_k = [d_{k,1}, d_{k,2}, d_{k,3}, d_{k,4}, d_{k,5}, d_{k,6}]^T$, which needs to be updated to enforce position and velocity continuity between sucessive intervals (similar to a multiple shooting method). Moreover, the hovering constraints are enforced at N_{hov} instants for each interval k (the enforcement period is $\Delta t_{\text{hov}} = \Delta t / N_{\text{hov}}$).

Following Ref. [18], a compact formulation is employed. Define the following stack vectors

$$\mathbf{d_S} = \begin{bmatrix} \mathbf{d}_1^T & \dots & \mathbf{d}_N^T \end{bmatrix}^T, \quad \Delta\mathbf{V_S} = \begin{bmatrix} \Delta\mathbf{V}_1^T & \dots & \Delta\mathbf{V}_N^T \end{bmatrix}^T, \tag{14}$$

$$\mathbf{x_S} = \begin{bmatrix} \mathbf{x}_{1,1} & \dots & \mathbf{x}_{1,N_{\text{hov}}} & \dots\dots & \mathbf{x}_{N,N_{\text{hov}}} \end{bmatrix}^T, \tag{15}$$

and the following stack matrix

$$\mathbf{G} = \begin{bmatrix} \mathbf{g}_{1,1} & \mathbf{0} & \dots & \mathbf{0} \\ \vdots & \vdots & \ddots & \vdots \\ \mathbf{g}_{1,N_{\text{hov}}} & \mathbf{0} & \dots & \mathbf{0} \\ \mathbf{0} & \mathbf{g}_{2,1} & \dots & \mathbf{0} \\ \vdots & \vdots & \ddots & \vdots \\ \mathbf{0} & \mathbf{g}_{2,N_{\text{hov}}} & \dots & \mathbf{0} \\ \mathbf{0} & \mathbf{0} & \dots & \mathbf{g}_{N,1} \\ \vdots & \vdots & \ddots & \vdots \\ \mathbf{0} & \mathbf{0} & \dots & \mathbf{g}_{N,N_{\text{hov}}} \end{bmatrix}, \tag{16}$$

Except where otherwise noted, content of this paper is licensed under a Creative Commons Attribution 4.0 International License.

The reproduction and distribution with attribution of the entire paper or of individual pages, in electronic or printed form, including some materials under non-CC-BY 4.0 licenses is hereby granted by the respective copyright owners.

where

$$\mathbf{g}_{k,j} = \begin{bmatrix} \mathbf{v}_{k,1}^T e^{\lambda_{k,1}\Delta t_j} \\ \mathbf{v}_{k,2}^T e^{\lambda_{k,2}\Delta t_j} \\ \mathbf{v}_{k,3}^T \cos(\omega_{k,1}\Delta t_j) - \mathbf{v}_{k,4}^T \sin(\omega_{k,1}\Delta t_j) \\ \mathbf{v}_{k,4}^T \cos(\omega_{k,1}\Delta t_j) + \mathbf{v}_{k,3}^T \sin(\omega_{k,1}\Delta t_j) \\ \mathbf{v}_{k,5}^T \cos(\omega_{k,2}\Delta t_j) - \mathbf{v}_{k,6}^T \sin(\omega_{k,2}\Delta t_j) \\ \mathbf{v}_{k,6}^T \cos(\omega_{k,2}\Delta t_j) + \mathbf{v}_{k,5}^T \sin(\omega_{k,2}\Delta t_j) \end{bmatrix}^T, \tag{17}$$

with $k = 1 \ldots N$, $j = 1 \ldots N_{\text{hov}}$ and $\Delta t_j = j\Delta t_{\text{hov}}$. The state propagation can be expressed as

$$\mathbf{x_S} = \mathbf{G}\mathbf{d_S}. \tag{18}$$

An idea to maintain the follower orbiting around the leader could be to cancel the unstable mode associated to d_1 as it is done under Keplerian assumptions (see Ref. [11]). Note that Eq. (18) does not guarantee position/velocity continuity between adjacent intervals k. The optimization problem (13) becomes

$$\begin{aligned} \min_{\mathbf{d_S}, \Delta\mathbf{V_S}} \quad & ||\Delta\mathbf{V_S}||_1, \\ \text{s.t.} \quad & \mathbf{A}_{\mathbf{S},\text{hov}}\mathbf{G}\mathbf{d_S} \leq \mathbf{b}_{\mathbf{S},\text{hov}}, \\ & (\mathbf{A}_{\mathbf{S},\mathbf{x}^+} - \mathbf{A}_{\mathbf{S},\mathbf{x}^-})\mathbf{G}\mathbf{d_S} = \mathbf{B_S}\Delta\mathbf{V_S}, \\ & \mathbf{A}_{\mathbf{x}_0}\mathbf{G}\mathbf{d_S} + \mathbf{B}_{\mathbf{x}_0}\Delta\mathbf{V_S} = \mathbf{x}_0, \\ & \mathbf{A}_{d_1}\mathbf{d_S} = \mathbf{0}, \\ & -\overline{\Delta\mathbf{V}}_\mathbf{S} \leq \Delta\mathbf{V_S} \leq \overline{\Delta\mathbf{V}}_\mathbf{S}, \end{aligned} \tag{19}$$

where $\mathbf{A}_{\mathbf{S},\text{hov}} \in \mathbb{R}^{6N_{\text{hov}}N \times 6N_{\text{hov}}N}$, $\mathbf{b}_{\mathbf{S},\text{hov}} \in \mathbb{R}^{6N_{\text{hov}}N}$ stack the hovering region matrix and vector inequalities. The position and velocity continuity (update of the $\mathbf{d}_k$ parameters) between adjacent intervals is imposed with the aid of the matrices $\mathbf{A}_{\mathbf{S},\mathbf{x}^+} \in \mathbb{R}^{6(N-1)\times 6N_{\text{hov}}N}$ and $\mathbf{A}_{\mathbf{S},\mathbf{x}^-} \in \mathbb{R}^{6(N-1)\times 6N_{\text{hov}}N}$ which extract the state before, $\mathbf{x}^-$, and after, $\mathbf{x}^+$, an impulse $\Delta\mathbf{V}$ is applied and the solution parameters changes. The matrix $\mathbf{A}_{d_1}$ assures cancellation of the unstable mode ($d_{k,1} = 0$) each time an impulse is applied. The compact optimization problem (19) can be easily recasted to an LP form by doing $\Delta\mathbf{V_S} = \Delta\mathbf{V_S}^+ - \Delta\mathbf{V_S}^-$, $\Delta\mathbf{V_S}^+ \geq \mathbf{0}$ and $\Delta\mathbf{V_S}^- \geq \mathbf{0}$.

5 Numerical results

In this section, a practical case with a target located in an Earth-Moon L_2 southern NRHO is considered. This orbit (see Fig. (2)) is the same as the one employed in Ref. [9] and has a period of $T_{\text{orb}} = 10.35$ days, a stability index of $\nu = 1.0120$ and a perilune of 17411 km. The Earth-Moon system parameters are $D = 384400$ km, $\mu_1 = 398600.4$ km^3/s^2 and $\mu_2 = 4904.869$ km^3/s^2. The time variable is changed to the phase angle (see Ref. [6]) as $\theta = 2\pi t/T_{\text{orb}}$. The origin of the angle ($\theta = 0$) is the orbit perilune.

All the simulations are done in MATLAB, with an i7-8700 3.2 GHz CPU, using both the non-linear CRTBP dynamics (see Eq. (1)) for the leader and the relative dynamics of Eq. (2) for the follower.

5.1 Propagation accuracy

Three linear propagation models are tested to assess their accuracy and numerical efficiency. The first one is based on the STM integration of Section 3.1. The others are based on the zero-order hold approach of Section 3.2 updating the target position at $\{\theta_{k-1}\}$ for ZOH1 and at $\{\theta_{k-1} + \Delta\theta/2\}$ for ZOH2 (being now $\Delta\theta$ the propagation interval duration).

Except where otherwise noted, content of this paper is licensed under a Creative Commons Attribution 4.0 International License.

The reproduction and distribution with attribution of the entire paper or of individual pages, in electronic or printed form, including some materials under non-CC-BY 4.0 licenses is hereby granted by the respective copyright owners.

Table 1 Root mean square position error along the trajectory for perilune flyby.

	Root mean square position error			Maximum position error		
N	ZOH1 (m)	ZOH2 (m)	STM (m)	ZOH1 (m)	ZOH2 (m)	STM (m)
1	317.24	1154.1	10.6724	780.09	3009.2	31.2048
10	44.6544	13.4254	10.6365	76.9642	38.4054	31.2048
40	14.8802	10.8125	10.6372	33.1108	31.6636	31.2048
100	11.1679	10.6651	10.6374	30.4394	31.2773	31.2048

Table 2 Propagation computation times for perilune flyby.

N	ZOH1 (ms)	ZOH2 (ms)	STM (ms)
1	4.1887	3.9015	775.17
10	7.8484	7.7000	817.16
40	15.6072	15.0981	864.01
100	27.7053	26.8562	1181.2

Two metrics are employed to effectively measure the propagation models accuracy. The first one is based on the root mean square error

$$\mathrm{RMS}_{\boldsymbol{\rho}} = \sqrt{\frac{1}{\theta_f - \theta_0}\int_{\theta_0}^{\theta_f} ||\boldsymbol{\rho} - \boldsymbol{\rho}_{\mathrm{NL}}||_2^2 d\theta}, \tag{20}$$

where NL stands for non-linear model. The second indicator is the maximum position error as

$$\mathrm{maxerr}_{\boldsymbol{\rho}} = \max(||\boldsymbol{\rho} - \boldsymbol{\rho}_{\mathrm{NL}}||_2^2). \tag{21}$$

5.1.1 Perilune flyby

Firstly, let evaluate a natural relative trajectory in the perilune region with $\{\theta_0 = -17.5^\circ, \theta_f = 17.5^\circ\}$, which roughly accounts for one day of propagation, and $\mathbf{x}_0 = [400, 300, 100, 0, 0, 0]^T$ m. The parameter under study is the number of zero-order hold intervals along the trajectory N (in the case of the STM model is the number of initial conditions updates). Table 1 shows the RMS position error and maximum error, with respect to N, for each considered model. As more updates are done, the accuracy of each method improves. The STM model shows no significant improvement as its initial condition is updated more (this is logical since $\boldsymbol{\Phi}(t_2, t_0) = \boldsymbol{\Phi}(t_2, t_1)\boldsymbol{\Phi}(t_1, t_0)$). However, ZOH1 and ZOH2 models improve their accuracy significantly until stalling. In all cases, ZOH2 provides a better accuracy than ZOH1. Note that the zero-order hold method yields a similar performance to the STM one for $N \geq 40$. Table 2 provides the computation time for each method. As expected, the computational burden augments as the discretization N increases. However, for the highest N, the ZOH1 and ZOH2 methods reduce the computational time by two orders of magnitude with respect to the STM model. The trajectory projection on the $\Delta x \Delta y$ plane is shown in Fig. 3 for $N = 40$ (note that ZOH2 and STM trajectories practically coincide).

Except where otherwise noted, content of this paper is licensed under a Creative Commons Attribution 4.0 International License.

The reproduction and distribution with attribution of the entire paper or of individual pages, in electronic or printed form, including some materials under non-CC-BY 4.0 licenses is hereby granted by the respective copyright owners.

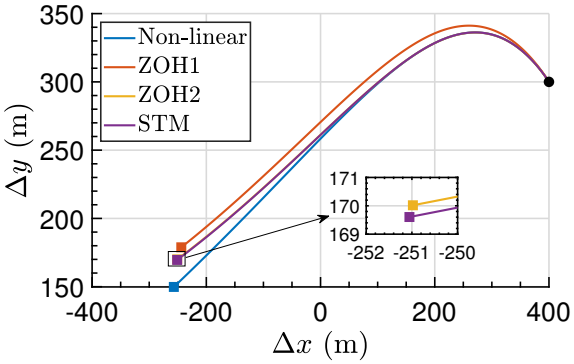

Fig. 3 Trajectories in the $\Delta x\Delta y$ plane for perilune flyby with $N = 40$.

Table 3 Root mean square position error along the trajectory for apolune flyby.

	Root mean square position error			Maximum position error		
N	ZOH1 (m)	ZOH2 (m)	STM (m)	ZOH1 (m)	ZOH2 (m)	STM (m)
1	0.8317	0.6631	0.0018	2.1970	1.0983	0.0042
10	0.1405	0.0075	0.0023	0.3175	0.0142	0.0058
40	0.0357	0.0025	0.0024	0.0811	0.0073	0.0069
100	0.0141	0.0024	0.0024	0.0326	0.0072	0.0071

5.1.2 Apolune flyby

Now, evaluate a natural trajectory in the vicinity of the apolune with $\{\theta_0 = 162.5°, \theta_f = 197.5°\}$ and $\mathbf{x}_0 = [400, 300, 100, 0, 0, 0]^T$ m. Table 3 shows the evolution of the RMS position error and the maximum error, with respect to N, for each considered model. Similar conclusions to the perilune case yield. However, note that the accuracies are far better when compared to perilune (see Table 1). This is caused by a faster dynamics behaviour near the perilune compared to the apolune. Table 4 provides the computation time for each method. The zero-order hold method is again more efficient computationally than the state transition matrix computation. The trajectory projection in the $\Delta x\Delta y$ plane is shown in Fig. 4 for $N = 40$ (note that all the trajectories coincide at practical effects).

5.1.3 Dynamics along the NRHO

The pure part of the state matrix $\mathbf{A}$ eigenvalues along the NRHO are represented in Fig. 5(a) (real part) and Fig. 5(b) (imaginary part) respectively. The previously mentioned stable-unstable and os-

Table 4 Propagation computation times for apolune flyby.

N	ZOH1 (ms)	ZOH2 (ms)	STM (ms)
1	3.5343	3.3629	122.742
10	8.1387	7.4960	162.545
40	18.6072	18.1182	360.275
100	30.5167	30.7559	750.243

Except where otherwise noted, content of this paper is licensed under a Creative Commons Attribution 4.0 International License.

The reproduction and distribution with attribution of the entire paper or of individual pages, in electronic or printed form, including some materials under non-CC-BY 4.0 licenses is hereby granted by the respective copyright owners.

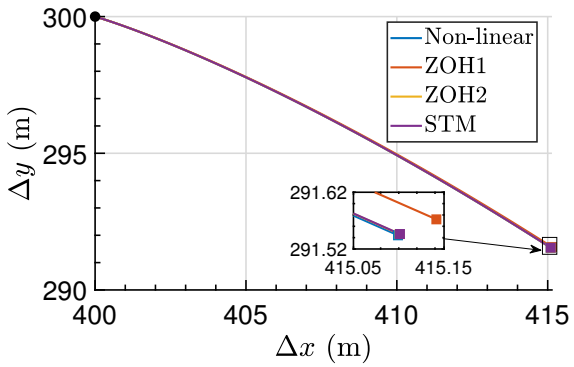

Fig. 4 Trajectories in the $\Delta x\Delta y$ plane for apolune flyby with $N = 40$.

cillatory behaviour (see Eq. (10)) is demonstrated. Moreover, the highest unstable mode and natural frequencies arise at the perilune (this explains its faster dynamics).

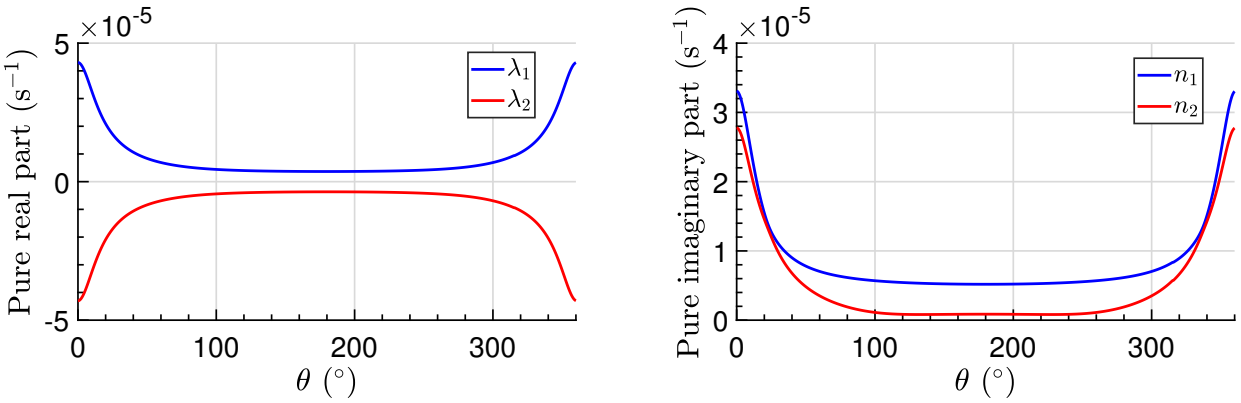

Fig. 5 Real part of pure real state matrix eigenvalues along the NRHO (a); imaginary part of pure imaginary state matrix eigenvalues along the NRHO (b).

5.2 Hovering phase control

Now, the ZOH2 propagation model is employed to impulsively control a hovering phase. The cuboid is defined as $\{\underline{\Delta x} = -400, \overline{\Delta x} = 400, \underline{\Delta y} = 200, \overline{\Delta y} = 400, \underline{\Delta z} = -300, \overline{\Delta z} = 300\}$ m and the impulse amplitude limited by $\overline{\Delta \mathbf{V}} = [2,2,2]^T$ cm/s. The follower is assumed to depart within the hovering zone with $\boldsymbol{\rho}_0 = [0,300,0]^T$ m and $\dot{\boldsymbol{\rho}}_0 = \mathbf{0}$ m/s. The target is initially placed at the perilune, $\theta_0 = 0$. The controller parameters are chosen as $N = 40$ and $N_{\text{hov}} = 4$ with a control horizon of $\theta_{f,k} - \theta_{0,k} = 36°$. At the end of each propagation interval, Δt, the control sequence is updated by solving the LP problem of (19). The simulation lasts for ten leader orbital periods (103.5 days). Figure 6(a) shows the relative trajectory for the hovering phase demonstrating the effectiveness of algorithm. The follower remains within the hovering region the 96.68% of time (the maximum constraint violation is of 1.5366 m) which is caused by the linear control model and the discrete constraints enforcement. Figure 6(b) shows the applied impulses along the trajectory. The total mission cost is of 3.7785 m/s. A strong correlation between the control effort and the perilune region can be observed. This is logical since Fig. 5 has demonstrated the faster dynamics behaviour at perilune. The control sequence computation time takes in average 0.0636 s with a peak of 0.1583 s.

Except where otherwise noted, content of this paper is licensed under a Creative Commons Attribution 4.0 International License.

The reproduction and distribution with attribution of the entire paper or of individual pages, in electronic or printed form, including some materials under non-CC-BY 4.0 licenses is hereby granted by the respective copyright owners.

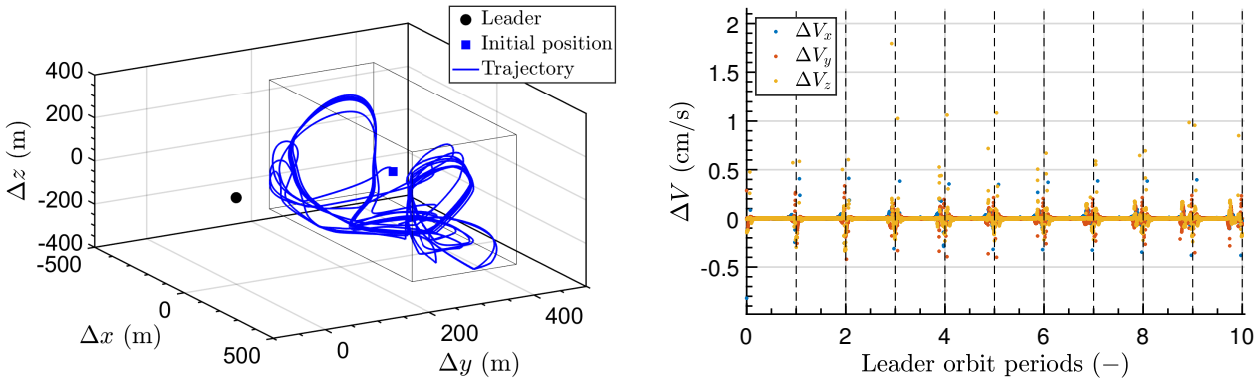

Fig. 6 Hovering phase trajectory (a); velocity increments (b).

6 Conclusions

A novel propagation method for the CRTBP relative dynamics has been presented. This technique is based on assuming the system as LTI for the propagation horizon and obtaining the solution in terms of the state matrix eigendecomposition. When compared to the alternate approach of computing the STM through numerical integration, the proposed approach provides a higher computational efficiency with almost the same accuracy.

Additionally, the zero-order hold method has been employed to solve the spacecraft rendezvous hovering phase in the context of the CRTBP. By studying the linear solution structure, the control strategy aims at cancelling the unstable mode. However, the constraints are enforced in a discrete way which does not guarantee its satisfaction between enforcement times. Future work may include the use of polynomial positiveness techniques (see Ref. [19]) to assure constraints satisfaction in a continuous way.

Acknowledgments

The authors gratefully acknowledge financial support from Universidad de Sevilla, through its V-PPI US, and grant PGC2018-100680-B-C21 funded by MCIN/AEI/10.13039/501100011033.

References

[1] M. Merri and M. Sarkarati. Lunar Orbiter Platform - Gateway: a clear use case for CCSDS MO services. In *2018 AIAA SPACE and Astronautics Forum and Exposition*, Orlando, Florida, United States of America, June 2018. DOI: https://doi.org/10.2514/6.2018-5337.

[2] R. Whitley and R. Martinez. Options for staging orbits in cislunar Space. In *2016 IEEE Aerospace Conference*, Big Sky, Montana, United States of America, March 2016. DOI: https://doi.org/10.1109/AERO.2016.7500635.

[3] P. Hayne, A. Hendrix, E. Sefton-Nash, M. Siegler, P.G. Lucey, K. Retherford, J. Williams, B.T. Greenhagen, and D.A. Paige. Evidence for exposed water ice in the Moon's south polar regions from Lunar Reconnaissance Orbiter ultraviolet albedo and temperature measurements. *Icarus*, 255(15):58–69, 2015. DOI: 10.1016/j.icarus.2015.03.032.

Except where otherwise noted, content of this paper is licensed under a Creative Commons Attribution 4.0 International License.

The reproduction and distribution with attribution of the entire paper or of individual pages, in electronic or printed form, including some materials under non-CC-BY 4.0 licenses is hereby granted by the respective copyright owners.

[4] E.M. Zimovan, K.C. Howell, and D.C. Davis. Near Rectilinear Halo Orbits and their Application in Cis-Lunar Space. In *3rd IAA Conference on Dynamics and Control of Space Systems*, Moscow, Russia, May 2017.

[5] G. Gomez, W. S. Koon, M. W. Lo, J. E. Marsden, J. Masdemont, and S. D. Ross. Connecting orbits and invariant manifolds in the spatial restricted three-body problem. *Nonlinearity*, 17(5):1571–1606, 2004. DOI: http://dx.doi.org/10.1088/0951-7715/17/5/002.

[6] Y. Sato, K. Kitamura, and T. Shima. Spacecraft Rendezvous Utilizing Invariant Manifolds for a Halo Orbit. *Transactions of the Japan Society for Aeronautical and Space Sciences*, 58(5):261–269, 2015. DOI: https://doi.org/10.2322/tjsass.58.261.

[7] G. Franzini and M. Innocenti. Relative motion equations in the local-vertical local-horizontal frame for rendezvous in lunar orbits. In *2017 AAS/AIAA Astrodynamics Specialist Conference*, Stevenson, Washington, United States of America, August 2017.

[8] S. Lizy-Destrez, L. Beauregard, E. Blazquez, A. Campolo, S. Manglativi, and V. Quet. Rendezvous Strategies in the Vicinity of Earth-Moon Lagrangian Points. *Frontiers in Astronomy and Space Sciences*, 5(45):1–19, 2019. DOI: https://doi.org/10.3389/fspas.2018.00045.

[9] J.C. Sanchez, F. Gavilan, and R. Vazquez. Chance-constrained Model Predictive Control for Near Rectilinear Halo Orbit spacecraft rendezvous. *Aerospace Science and Technology*, 100:105827, May 2020. DOI: 10.1016/j.ast.2020.105827.

[10] D. J. Irvin, R. G Cobb, and T. A. Lovell. Fuel-optimal maneuvers for constrained relative satellite orbits. *Journal of guidance, control, and dynamics*, 32(3):960–973, 2009. DOI: https://doi.org/10.2514/1.36618.

[11] P.R. Arantes-Gilz, M. Joldes, C. Louembet, and F. Camps. Stable model predictive strategy for rendezvous hovering phases allowing for control saturation. *Journal of Guidance, Control, and Dynamics*, 42(8):1658–1675, 2019. DOI: https://doi.org/10.2514/1.G003558.

[12] Louis Breger and Jonathan P. How. Safe Trajectories for Autonomous Rendezvous of Spacecraft. *Journal of Guidance, Control and Dynamics*, 31(5):1–8, 2008. DOI: https://doi.org/10.2514/1.29590.

[13] S. Di Cairano, H. Park, and I. Kolmanovsky. Model Predictive Control approach for guidance of spacecraft rendezvous and proximity maneuvering. *International Journal of Robust and Nonlinear Control*, 22(12):1398–1427, 2012.

[14] X. Yang and X. Cao. A new approach to autonomous rendezvous for spacecraft with limited impulsive thrust: Based on switching control strategy. *Aerospace Science and Technology*, 43:454–462, June 2015.

[15] E.J. Doedel, R.C. Paffenroth, H.B. Keller, D.J. Dichmann, J. Galan-Vioque, and A. Vanderbauwhede. Computation of Periodic Solutions of Conservative Systems with Application to the 3-Body Problem. *International Journal of Bifurcation and Chaos*, 13(6):1353–1381, 2003. DOI: https://doi.org/10.1142/S0218127403007291.

[16] K. Yamanaka and F. Ankersen. New State Transition Matrix for Relative Motion on an Arbitrary Elliptical Orbit. *Journal of Guidance, Control and Dynamics*, 25(1):60–66, 2002. DOI: https://doi.org/10.2514/2.4875.

[17] E.F. Camacho and C. Bordons. *Model Predictive Control*, chapter 9, pages 249–287. Springer-Verlag, London, 2 edition, 2004. DOI: https://doi.org/10.1007/978-0-85729-398-5.

[18] F. Gavilan, R. Vazquez, and E.F. Camacho. Chance-constrained model predictive control for spacecraft rendezvous with disturbance estimation. *Control Engineering Practice*, 60:111–122, 2012. DOI: https://doi.org/10.1016/j.conengprac.2011.09.006.

[19] G. Deaconu, C. Louembet, and A. Théron. Designing continuously constrained spacecraft relative trajectories for proximity operations. *Journal of Guidance, Control, and Dynamics*, 38(7):1208–1217, 2015.

Except where otherwise noted, content of this paper is licensed under a Creative Commons Attribution 4.0 International License.

The reproduction and distribution with attribution of the entire paper or of individual pages, in electronic or printed form, including some materials under non-CC-BY 4.0 licenses is hereby granted by the respective copyright owners.